

# Motron: Multimodal Probabilistic Human Motion Forecasting

Tim Salzmann  
 Technical University Munich  
 tim.salzmann@tum.de

Marco Pavone  
 Stanford University  
 and NVIDIA Research  
 pavone@stanford.edu

Markus Ryll  
 Technical University Munich  
 markus.ryll@tum.de

## Abstract

*Autonomous systems and humans are increasingly sharing the same space. Robots work side by side or even hand in hand with humans to balance each other’s limitations. Such cooperative interactions are ever more sophisticated. Thus, the ability to reason not just about a human’s center of gravity position, but also its granular motion is an important prerequisite for human-robot interaction. Though, many algorithms ignore the multimodal nature of humans or neglect uncertainty in their motion forecasts. We present Motron, a multimodal, probabilistic, graph-structured model, that captures human’s multimodality using probabilistic methods while being able to output deterministic motions and corresponding confidence values for each mode. Our model aims to be tightly integrated with the robotic planning-control-interaction loop; outputting physically feasible human motions and being computationally efficient. We demonstrate the performance of our model on several challenging real-world motion forecasting datasets, outperforming a wide array of generative methods while providing state-of-the-art deterministic motions if required. Both using significantly less computational power than state-of-the-art algorithms.*

## 1. Introduction

The key desideratum of autonomous systems is to provide added value to humans while ensuring safety. Traditionally, safety aspects limit such robots to low-risk tasks with minimal human interaction. An understanding of humans and their distribution of feasible and anticipated movement is key to develop safe, risk-aware human-interactive autonomous systems. Such systems could operate in closer proximity to humans, performing tasks involving higher levels of interaction, providing enhanced added value. Fig. 1 illustrates a handover scenario where predicting the human’s motion is key to the autonomous system’s task and trajectory planning.

However, capturing the complexity of human motion in a computational model is challenging due to the multitude of continuous movement possibilities (multimodality), even within fixed boundaries of physical limitations. Tra-

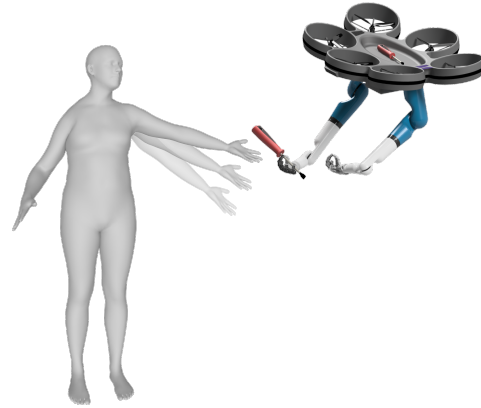


Figure 1. Exemplary scenario of a drone handing over an object to a human. Predicting the human’s motion is key to a successful interaction during all stages of the maneuver.

ditionally, over-conservative systems rely solely on those constraints to ensure safety, while deterministic predictive methods discard the potential of many high-level futures in favor of a single possible motion.

In contrast to such deterministic regressors, generative models aim to produce samples of human future motion. However, for different reasons (e.g., simulation purposes), they prioritize generative diversity over representing actual plausible motions. For robotic use cases, we aim for samples to represent the underlying distribution of possible motions; or even better a parametric description thereof.

Both, deterministic and generative, human motion predictions have been developed independently to maximize their strengths in accuracy and diversity. Still, many of them have been developed without directly accounting for real-world robotic use cases; they settle for diversity instead of accuracy, ignore physical boundaries, and are computationally too expensive.

We target robotic use cases, where predictions are used in a control loop. As such, a model has to capture the underlying distribution of possible human motions without being over-confident or over-diverse within an imminent time horizon; *combining* and *balancing* the desiderata of both research strands. In consequence, we are interested in developing a human motion prediction model that (I) represents the inherent multimodal structure of human motion;

(II) accurately captures humans’ probabilistic and diverse nature while obeying kinematic constraints; (III) by directly incorporating structural information of the human skeleton; (IV) while being able to deal with imperfect data; (V) outputting the maximum amount of information for the use of subsequent systems.

To achieve those desiderata, our contribution is threefold: First, we describe a new efficient way to model graph-structured problems where nodes have a fixed semantic class, usable for generic graph-structured problems. Secondly, we present *Motron*, which uniquely uses a probabilistic output structure based on the Concentrated Gaussian distribution in SO3 and a parallel weight sharing approach incorporating the skeleton’s structure. It is designed to mirror the multimodal and uncertain nature of humans. To the best of our knowledge, this is the first algorithm capable of producing a parametric distribution over future human skeleton configurations. *Motron*’s flexible output structure is designed to serve downstream robotic modules such as motion planning, decision making, and control. Finally, we evaluate our model on the fulfillment of our desiderata using deterministic and generative metrics; combining both research strands. We outperform an extensive selection of generative motion prediction methods while showing state-of-the-art performance on deterministic evaluation procedures using a variety of metrics and datasets. Our contributions are substantiated by a thorough ablation study. We further show that *Motron* can deal with occluded data often present in real-world applications by including the additional uncertainty in its output.

## 2. Related Work

**Human Motion Forecasting.** The release of the H3.6M dataset [19] in 2014 stimulated a wealth of research in the field of human motion prediction. While early works were based on traditional approaches such as Markov Models [31,40] or Gaussian Processes [48] the advances of deep learning has taken over recent approaches. Results are now largely based on deterministic regressors [10, 11, 37, 39]; improving performance by incorporating human skeleton structural information into their architectures [22, 32]. Li *et al.* [32] merge nodes to create meta graphs of different scale to extract higher level information. Within those, two concepts of capturing temporal influences have emerged: Recurrent Neural Networks (RNNs) and transforming time-series to a frequency domain using discrete cosine transformation [34, 53], where the latter is not agnostic to varying history horizons. Recently, Transformer [45] architectures have been explored overcoming RNNs shortcomings in capturing longer time series [34, 43]. While generative approaches have emerged as state-of-the-art in trajectory forecasting [26, 42, 44] for their plethora of captured information, they largely exist in parallel to research on deterministic regressors in human motion forecasting. The field is split in approaches using Generative Adversarial Networks (GANs) [3, 16, 17, 27] and (Conditional) Variational Autoen-

Table 1. A summary of recent state-of-the-art human motion forecasting methods and their addressed desiderata.

Method	G	P	C	DTH	CF	OS
AGED [16]			✓	✓		
DMGMM [32]			✓	✓		✓ <sup>1</sup>
DLow [52]	✓			✓	✓	✓ <sup>2</sup>
LCP-VAE [1]	✓			✓	✓	? <sup>3</sup>
HistRepItself [34]			✓		✓	✓ <sup>4</sup>
Our Work	✓	✓	✓	✓	✓	✓

Legend: G = Generative, P = Probabilistic Output, C = Adheres to kinematic constraints, DTH = Dynamic Time Horizon, CF = Computationally Feasible, OS = Open Source

coders ((C)VAEs) [51–53]. Of these, similar to the field of trajectory prediction, adapted versions of the VAE frameworks show better results [52].

Surprisingly, these two fields of deterministic and generative motion prediction are highly disentangled, following their respective distinct experimentation protocols. In deterministic setups, it is, for example, common to predict one second into the future. In contrast, previous generative works set their focus on producing plausible diverse motions over a longer prediction horizon (2s); at which point the true human motion is fraught with uncertainty.

**Directional Probabilistic Learning.** In robotic applications, such as filtering, the use of directional statistics for rotational systems has been proven useful [12, 14, 28, 29]. The most common distributions for modeling rotational uncertainty are the Bingham [5], the von Mises–Fisher [9], the Projected Gaussian [30], and using a Concentrated Gaussian in SO(3) [2, Chapter 7.3.1]. Advances in deep probabilistic learning, however, are mainly focused on learning distributions in vector space [6, 7, 42]. Thus, of the rotational distributions, only the Bingham distribution has been applied to probabilistic deep learning [13, 41]. In [13] Gilitschenski *et al.* directly learn the parameters of a Bingham distribution representing the orientation of an object in an image. To the best of our knowledge, there is no approach leveraging probabilistic learning within the field of human motion prediction.

**Graph Neural Networks.** Besides other concepts like message passing, convolution, and aggregation [54] the concept of attention, first introduced for temporal dependencies [45], has been applied to graph-structured problems by Veličković *et al.* [46] as Graph Attention Networks (GAT). Recently those GATs have been included in temporal networks such as LSTMs by replacing the linear transformations in each RNN cell with a Graph Attention Layer [49]. Within human motion forecasting Graph Convolution Networks (GCNs) [34, 35] have shown good performance. Salzman *et al.* [42] model dependencies between different entities for trajectory prediction using a sequential message passing algorithm. This, however, becomes computational infeasible for larger number of node types.

<sup>2</sup><https://github.com/limaosen0/DMGNN>

<sup>3</sup><https://github.com/Khrylx/DLow>

<sup>4</sup>Not openly accessible (yet) at time of submission.

<sup>5</sup><https://github.com/wei-mao-2019/HisRepItself>

Tab. 1 provides a detailed breakdown of recent state-of-the-art approaches and their consideration of desiderata.

### 3. Problem Formulation

We aim to generate plausible motion distributions for a fixed number  $N$  of human skeleton nodes (joints)  $n_1, \dots, n_N$ . Each node  $n_i$  is assigned to a semantic class  $S_i$ , e.g. Elbow, Knee, or Hip. At time  $t$ , given the  $D$ -dimensional state  $\mathbf{s} \in \mathbb{R}^D$  of each node and all of their histories for the previous  $H$  timesteps, which we denote as  $\mathbf{x} = \mathbf{s}_{1, \dots, N}^{(t-H:t)} \in \mathbb{R}^{(H+1) \times N \times D}$ , we seek a distribution over all nodes' future states for the next  $T$  timesteps  $\mathbf{y} = \mathbf{s}_{1, \dots, N}^{(t+1:t+T)} \in \mathbb{R}^{T \times N \times D}$ , which we denote as  $p(\mathbf{y} | \mathbf{x})$ .

### 4. Preliminaries

**Quaternion Representation.** The rotational nature of the human anatomy presents a challenge to neural networks. Commonly used rotation representations in  $\mathbb{R}^3$ , Euler angles and exponential maps, suffer from singularities, discontinuity, and non-uniqueness [15, 39]; all properties contrary to neural network characteristics. Outside of deep learning, however, quaternions have long been established as the default rotational representation. As a consequence of their properties, interpretability, and common use in robotics we choose quaternions as the data representation throughout our model. Thus the input state  $\mathbf{x}_i^{(t)} = [\mathbf{q}_i^{(t)}, \dot{\mathbf{q}}_i^{(t)}]$  is defined as the concatenation of the rotation in quaternion representation and its time differential, where  $\mathbf{q}_i^{(t)} = \mathbf{q}_i^{(t-1)} \odot \dot{\mathbf{q}}_i^{(t)}$ ; resulting in a  $D = 8$  dimensional state.

**Probabilistic Rotations.** We use the Concentrated Gaussian distribution  $\mathcal{N}_{SO(3)}$  [2, Chapter 7.3.1] to model a probability distribution over the rotation group  $SO(3)$ . A probabilistic rotation is given as

$$\mathbf{R} = \exp(\hat{\epsilon})\bar{\mathbf{R}} \quad (1)$$

where  $\bar{\mathbf{R}}$  is a 'large', noise-free, nominal rotation,  $\exp$  is the exponential map,  $\hat{\cdot}$  is a linear, skew-symmetric Lie algebra operator, and  $\epsilon \in \mathbb{R}^3$  is a 'small', noisy component:

$$\epsilon \sim \mathcal{N}(\mathbf{0}, \Sigma) \quad (2)$$

The distribution's *p.d.f* is defined as

$$p(\mathbf{R} | \bar{\mathbf{R}}, \Sigma) = \frac{1}{Z} e^{-\frac{1}{2}(\ln(\mathbf{R}\bar{\mathbf{R}}^T) \cdot)^T \Sigma^{-1} (\ln(\mathbf{R}\bar{\mathbf{R}}^T) \cdot)} \quad (3)$$

where  $Z$  is the Gaussian normalization constant,  $\ln$  is the inverse of the exponential map, and  $\cdot$  is the inverse linear, skew-symmetric Lie algebra operator.

Unlike the Bingham or Von Mises-Fisher, the Concentrated Gaussian distribution supports the analytical composition of rotations which is a necessary property as we use differential quaternions as intermediate output representation (this is justified in Sec. 6.2.1). A probabilistic multiplication of two rotations  $\mathbf{R}_3 = \mathbf{R}_1\mathbf{R}_2$  is expressed as

$$\mathbf{R}_3 = \mathbf{R}_1\mathbf{R}_2 = \exp(\hat{\epsilon}_1)\bar{\mathbf{R}}_1\exp(\hat{\epsilon}_2)\bar{\mathbf{R}}_2 \quad (4)$$

without approximation we have

$$\begin{aligned} \mathbf{R}_3 &= \exp(\hat{\epsilon}_1)\exp(\hat{(\bar{\mathbf{R}}_1\epsilon_2)})\bar{\mathbf{R}}_1\bar{\mathbf{R}}_2 \\ &= \exp(\hat{\epsilon}_1)\exp(\hat{\epsilon}_{12})\bar{\mathbf{R}}_3 \end{aligned} \quad (5)$$

using first order Baker-Campbell-Hausdorff approximation we get

$$\mathbf{R}_3 = \exp((\epsilon_1 + \epsilon_{12})\hat{\cdot})\bar{\mathbf{R}}_3 \quad (6)$$

$$\mathbf{R}_3 \sim \mathcal{N}_{SO(3)}(\bar{\mathbf{R}}_1\bar{\mathbf{R}}_2, \Sigma_1 + \bar{\mathbf{R}}_1\Sigma_2\bar{\mathbf{R}}_1^T) \quad (7)$$

To represent multimodality, we define our output structure as a Concentrated Gaussian Mixture Model in  $SO(3)$  ( $\mathcal{N}_{SO(3)}^\pi$ ). For  $q \sim \mathcal{N}_{SO(3)}^\pi(\pi_i, \bar{\mathbf{R}}_i, \Sigma_i)$ , the *p.d.f* is given as

$$p(\mathbf{R} | \pi, \bar{\mathbf{R}}, \Sigma) = \sum_i \pi_i \mathcal{N}_{SO(3)}(\bar{\mathbf{R}}_i, \Sigma_i) \quad (8)$$

where  $\pi_i \in \mathbb{R}$  is the mixture coefficient for the  $i$ -th  $\mathcal{N}_{SO(3)}$  component.

As quaternions  $\mathbf{q}$  and rotation matrices  $\mathbf{R}$  are interchangeable representations the Concentrated Gaussian distribution in  $SO(3)$  is implemented on a quaternion basis.

**Typed Graph Attention.** To make use of the information of the human skeleton, the entire model is comprised of two building blocks which preserve and efficiently resemble the skeleton structure. Both modules utilize a Graph Influence Matrix  $G \in \mathbb{R}^{N \times N}$  inspired by previous work [25, 32, 35]. Matrix multiplying the Graph Influence Matrix with a Graph State Matrix  $\mathbf{x} \in \mathbb{R}^{N \times D_I}$  calculates an element-wise weighted sum of each node's state. This operation is known as *Graph Convolution* [25] or *Graph Attention* [46] where the attention weights are learned instead of inferred from node states.

To allow for model particularities depending on the semantic class  $S_i$  of node  $n_i$ , we define a typed weight tensor  ${}^N\mathbf{W} \in \mathbb{R}^{N \times D_I \times D_O}$  as  $N$  stacked weight matrices  $\mathbf{W}_S \in \mathbb{R}^{D_I \times D_O}$  where  $\mathbf{W}_S$ :

$${}^N\mathbf{W} = [\mathbf{W}_{S_0} \quad \mathbf{W}_{S_1} \quad \dots \quad \mathbf{W}_{S_N}] \quad (9)$$

We define the multiplication operator  $\cdot$  as a batched matrix multiplication between the typed weight tensor  ${}^N\mathbf{W}$  and the graph input matrix  $\mathbf{x} \in \mathbb{R}^{N \times D_I}$

$$f(\mathbf{x}) = {}^N\mathbf{W} \cdot \mathbf{x} \quad (10)$$

All nodes  $n_i$  of the same type  $S_i$  share the same weights and all  $N$  nodes are processed with a single batched matrix multiplication allowing for efficient learning.

**Typed Graph (TG)-Linear:** Using both concepts, attention and typed weights, we define the equivalent to a linear fully connected layer in our graph neural network as

$$f(\mathbf{x}) = \mathbf{G}({}^N\mathbf{W} \cdot \mathbf{x}) \quad (11)$$

**Typed Graph (TG)-GRU:** To capture temporal dependencies within the model we introduce the typed graph equiva-

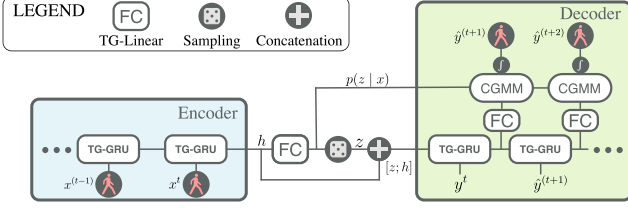


Figure 2. Our network architecture: The encoder abstracts human’s historic poses into a hidden representation  $h$  using a  $TG-GRU$ . This representation is used to infer the distribution over the latent variable  $p(z | \mathbf{x})$ , and is fed into the decoder together with latent samples  $z$ . The decoder, again, uses a  $TG-GRU$  to compute the output distribution. Notably,  $p(z | \mathbf{x})$  is reused as mixing coefficients in the output distribution.

lent to an GRU layer as

$$\begin{aligned}
 r_t &= \sigma_g(\mathbf{G}_t(N\mathbf{W}_r \cdot x_t) + \mathbf{G}_t(N\mathbf{U}_r \cdot h_{t-1}) + b_f) \\
 z_t &= \sigma_g(\mathbf{G}_t(N\mathbf{W}_z \cdot x_t) + \mathbf{G}_t(N\mathbf{U}_z \cdot h_{t-1}) + b_f) \\
 n_t &= \sigma_g(\mathbf{G}_t(N\mathbf{W}_n \cdot x_t) + r_t \circ \mathbf{G}_t(N\mathbf{U}_n \cdot h_{t-1}) + b_f) \\
 h_t &= (1 - z_t) \circ n_t + z_t \circ h_{t-1} \\
 \mathbf{G}_t &= \mathbf{G}_{t-1} + \mathbf{G}_{ta}
 \end{aligned}$$

where  $\mathbf{G}_0$ ,  $N\mathbf{W}$  and  $N\mathbf{U}$  are trainable parameters.  $h$  is the GRUs state and  $\sigma$  represents an activation function. The input  $x \in \mathbb{R}^{N \times D_I}$  holds  $D_I$  dimensional information on the  $N$  nodes. The Graph Influence Matrix  $\mathbf{G}$  is initialized as unit matrix and is optimized during training. For the  $TG-GRU$  an additional Temporal Additive Graph Influence Matrix  $G_{ta} \in \mathbb{R}^{N \times N}$  is initialized as a zero matrix and is optimized to capture the temporal change of influence between nodes over time.

## 5. Motron

Our model is visualized in Fig. 2. From a high-level perspective, we combine latent discrete variables with probabilistic mixture distribution as output structure to model the diverse nature of human motion while embedding the skeleton graph structure directly into the learning and inference procedure by using only *Typed Graph* components.

This model extends core concepts of probabilistic, multimodal deep learning towards the application of human motion prediction. We call our model *Motron*.

**Graph Structure Embodiment.** We enable efficient use of graph-structured information by imbuing the architecture from end to end. Thus, the architecture is fully described by the two building blocks  $TG-Linear$  and  $TG-GRU$ ; there is no fully connected influence between hidden node states. This leads to natural modeling of the information flow, where weights are shared between symmetric joints as well as a reduction in model parameters of about 40%.

**Modeling Motion History.** Starting from the input representation  $\mathbf{x} = \mathbf{s}_{1, \dots, N}^{(t-H:t)} \in \mathbb{R}^{H \times N \times D}$ , the model needs to encode a node’s current state and its history. To encode the observed history of the node, its current and previous states are fed into a  $TG-GRU$  network. The final output is encoded to the model’s hidden state  $h$  by a  $TG-Linear$  layer.

**Explicitly Accounting for Multimodality.** *Motron* explicitly handles multimodality by leveraging a probabilistic latent variable architecture loosely inspired by (*Conditional*) *Variational Autoencoders* ((C)VAEs). It produces the target distribution  $p(\mathbf{y} | \mathbf{x})$  by introducing a discrete latent variable  $z$ ,

$$p(z | x) = \frac{1}{N} \sum_i f_{TG-Linear}(h)_i, \quad (12)$$

which encodes high-level latent behavior and allows for  $p(\mathbf{y} | \mathbf{x})$  to be expressed as

$$p(\mathbf{y} | \mathbf{x}) = \sum_z p_\psi(\mathbf{y} | \mathbf{x}, z) p_\theta(z | \mathbf{x}), \quad (13)$$

where  $\psi$  and  $\theta$  are deep neural network weights that parameterize their respective distributions.

**Producing Motions.** The sampled latent variable  $z$  is concatenated with the hidden representation vector  $h$  and fed into our  $TG-GRU$  decoder. Each  $TG-GRU$  cell outputs the parameters  $\bar{\mathbf{R}}, \Sigma$  of a  $\mathcal{N}_{SO(3)}$  for each node. Using  $\pi_i = p(z = i | \mathbf{x})$  we produce the mixture model  $\hat{\mathbf{q}} \sim \mathcal{N}_{SO(3)}^\pi$  over differential quaternions as an intermediate output distribution.

Thus,  $z$  being discrete is necessary as it enables us to rethink Eq. (13) as a  $\mathcal{N}_{SO(3)}^\pi$  with mixture distribution  $p(z | x)$ . It also aids in interpretability, as one can visualize the high-level behaviors resulting from each  $z$  by sampling motions (see Fig. 4).

Using the closed composition formula Eq. (6) of the Concentrated Gaussian in  $SO(3)$  we can “integrate” the distribution over differential quaternions to the final output distribution over quaternions. The intermediate step is necessary as motion samples are produced by sampling differential quaternions and subsequently “integrating” them to motions. Directly sampling the output distribution would lead to time inconsistent motions. Additionally, using differential output for recurrent layers is known to ease the learning problem and improve convergence [21, 42].

**Training the Model.** Commonly, learning good representations for probabilistic latent variables is achieved by including the ground truth  $y$  as input to the latent layer during training and simultaneously introducing a *Kullback–Leibler Divergence* (KL) loss term to *squeeze* out the dependency on  $y$  during the training process [18, 42]. When using the CVAE framework, these competing conditions can lead to unstable training behavior and the collapse of the latent distribution (KL divergence towards zero). In contrast, we do not input the ground truth but give the model the option to use the latent capacity  $p_\theta(z | \mathbf{x})$  to maximize Eq. (13) in Eq. (14). Formally, we aim to solve

$$\max_{\theta, \psi} \sum_{i=1}^N \mathbb{E}_{z \sim p_\theta(\cdot | \mathbf{x}_i)} [\log p_\psi(\mathbf{y}_i | \mathbf{x}_i, z)] \quad (14)$$

Notably, no reparameterization trick, commonly needed for training probabilistic latent variable models [23, 24] is used to backpropagate through the categorical latent variable  $z$

as it is not sampled during training time. Instead, Eq. (14) is directly computed since the latent space has only  $|Z|$  discrete elements. (For a in depth discussion see Appendix A)

**Output Configurations.** Based on the desired use case, *Motron* can produce many different outputs. The main four are outlined below.

1. *Distribution:* Due to the use of a discrete latent variable and probabilistic output structure, the model can provide an analytic output distribution by directly computing Eq. (13). This parametric  $\mathcal{N}_{SO(3)}^\pi$  distribution entails the complete information inferred by the model.

2. *Sampled:* The model’s sampled output, where  $z$  and  $y$  are sampled sequentially according to

$$z \sim p_\theta(z | \mathbf{x}), \quad \mathbf{y} \sim p_\psi(\mathbf{y} | \mathbf{x}, z). \quad (15)$$

3. *Most Likely Mode (ML-Mode):* The model’s deterministic and most-likely single output. The high-level latent behavior mode and output trajectory are the modes of their respective distributions, where

$$\begin{aligned} z_{\text{mode}} &= \arg \max_z p_\theta(z | \mathbf{x}), \\ \mathbf{y} &= \arg \max_{\mathbf{y}} p_\psi(\mathbf{y} | \mathbf{x}, z_{\text{mode}}). \end{aligned} \quad (16)$$

4. *Weighted Mean (W-Mean)* The mean of all latent modes weighted by their probability. Following [36], it is given as the normalized largest eigenvector of  $QQ^T$  where  $Q$  is a matrix of stacked quaternion column vectors, where

$$\begin{aligned} \mathbf{q}_n &= \mathbf{y}_n = \arg \max_{\mathbf{y}} p(\mathbf{y} | \mathbf{x}, z = n), \\ Q &= [\pi_1 \mathbf{q}_1, \dots, \pi_{|Z|} \mathbf{q}_{|Z|}]. \end{aligned} \quad (17)$$

## 6. Experiments

While desiderata (III) and (V) in Sec. 1 are explicitly fulfilled by the embedded human structure and the use of a  $\mathcal{N}_{SO(3)}^\pi$  as output distribution, we conduct both quantitative and qualitative experiments to show that our method also succeeds in the remaining desiderata.

We, therefore, structure our experiments as follows: First, we show that *Motron* performs best in capturing humans’ probabilistic and diverse nature (II) by introducing a new probabilistic metric to the field of human motion prediction. Secondly, we highlight the learned multimodal structure (I) by evaluating deterministic outputs of high likelihood modes. Later we also give a visualization of how these modes manifest in distinct motions. Finally, we show that our approach can handle incomplete data (IV) in the form of occluded joints.

**Datasets.** We provide quantitative experimentation results on two datasets; namely the *Human 3.6 Million* (H3.6M) [19] dataset and the *Archive of Motion Capture as Surface Shapes* (AMASS) [33]. AMASS is a unified collection of 18 motion capture datasets totaling 13944 motion-sequences from 460 subjects performing a large variety of

actions. In comparison, the H3.6M dataset consists of 240 sequences from 8 subjects performing 15 actions each.

### 6.1. Generative Evaluation

**Metrics.** Generative approaches have been compared on the basis of a variety of metrics in position space, most prominent are Best-of-N metrics where  $N = 50$  motions are sampled from the generative model; the best metric value of these is reported. Such metrics, however, only present limited insights on a model’s output distribution as only a single motion of an arbitrary number  $N$  is evaluated. To fully assess an algorithm’s probabilistic capabilities, we propose an alternative evaluation methodology for generative algorithms where we measure the ability to accurately capture and reproduce the underlying uncertainty distribution of motions. To this point we adopt the *KDE-NLL* metric [20] to assess the method’s Negative Log-Likelihood (NLL) by fitting a probability distribution, using Kernel Density Estimate (KDE) [38], to output samples. Although *Motron* can compute its own log-likelihood, we apply the same evaluation methodology to maintain a directly comparable performance measure. As the NLL is unbounded, we clip it to a maximum value of 20 ( $\sim 2 * 10^{-7}\%$ ) in order to prevent single outliers from dominating. Still, to be comparable, we additionally follow the evaluation methodology of Yuan *et al.* [52]: We report the *Average Pairwise Distance* (APD) as a measure of sample diversity as well as the Best-of-N metrics *Average Displacement Error* (ADE), and *Final Displacement Error* (FDE) as measures of quality. Further, we report their Multi-Modal ADE and FDE metrics (MMADE and MMFDE). “Similar“ motions are grouped by using an arbitrary distance threshold at  $t = 0$  and the average metric over all these grouped motions is reported. As close poses at a single instance can, however, belong to entirely different motions (Appendix C), the KDE-NLL reports a more holistic representation of a model’s generative capabilities.

**Generative Baselines.** We focus on the current state-of-the-art generative algorithm (1) *DLow* [52] to compare our desiderata side to side. *DLow* uses an adapted VAE algorithm to generate samples without collapsing to a single mode. For the standard generative experiment methodology, we further report methods based on CVAEs: (2) *Pose-Knows* [47] and (3) *MT-VAE* [50]; GAN based (4) *DeLiGAN* [17] and diversity promoting methods (5) *Best-of-Many* [4], (6) *GMVAE* [8], and (7) *DSF* [51]. We were not able to compare to *LCP-VAE* [1] for a lack of open accessible source code.

**Evaluation Methodology.** In order to compare to other generative methods, which output motions solely in position space, we use the forward kinematic of the respective test subject to convert our joint configuration samples to joint positions. Predicting in configuration space and using human’s forward kinematic to produce motions in position space, ensures our motions to be kinematic feasible. However, they bring a disadvantage compared to ap-

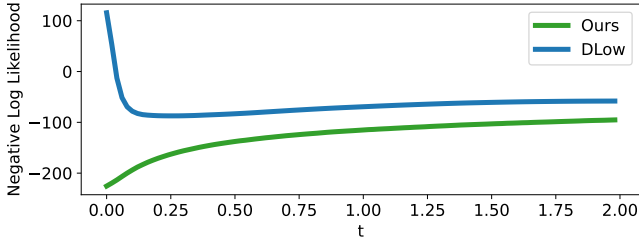


Figure 3. Negative Log Likelihood of the ground truth in the fitted KDE distribution of samples from each model. Lower is better. Samples from *DLow* are over-confidently wrong for early prediction timesteps.

	1 s			2 s		
	APD	ADE	FDE	APD	ADE	FDE
DSF [?]	-	-	-	9.330	0.493	0.592
DeLiGAN [17]	-	-	-	6.509	0.483	0.534
GMVAE [8]	-	-	-	6.769	0.461	0.555
Best-of-Many [4]	-	-	-	6.265	0.448	0.533
MT-VAE [50]	-	-	-	0.403	0.457	0.595
Pose-Knows [47]	-	-	-	6.723	0.461	0.560
<i>DLow</i> [52]	5.180	0.305	0.419	11.741	0.425	0.518
Ours	3.453	<b>0.252</b>	<b>0.350</b>	7.168	<b>0.375</b>	<b>0.488</b>

Table 2. Best of  $N = 50$  evaluation against generative algorithms on a prediction horizon of one and two seconds on H3.6M dataset.

proaches directly outputting joints positions, common for generative approaches, as they are not constrained by a rigid bone structure (Appendix D). For the KDE-NLL metric, we sample  $N = 1000$  motions from each method and fit a KDE for each future timestep. For the  $N = 50$  metrics (APD, ADE, FDE, MMADE, MMFDE) we use 50 motions, sampled from our intermediate output distribution over  $\dot{q}$  and "integrated"; these motions are transformed into position space using the respective subjects forward kinematics. We train the model on 0.5 seconds of history and predict a two second horizon. Generally, we can dynamically change the prediction horizon online thanks to the flexible decoder structure during inference.

**Results.** Fig. 3 shows that *Motron* clearly outperforms the current state-of-the-art algorithm *DLow* in representing the underlying motion distribution of the human subject and therefore having a lower NLL over all prediction timesteps. This result is supported by the Best-of-N metrics over one and two seconds in Tab. 2. We show significantly better results than *DLow* on ADE and FDE. Notably, this is achieved while using less diverse motion samples (lower APD) indicating that our samples are concentrated around likely motions. MMADE and MMFDE values for different thresholds are presented in Fig. 6 in Appendix C. For smaller thresholds we outperform *DLow* while for higher thresholds, where possibly uncorrelated motions are evaluated together as displayed in Fig. 7 in Appendix C, we unsurprisingly achieve lower scores as our approach does not over-diversify its predictions.

## 6.2. Deterministic Evaluation

**Metrics.** We report the *Mean Angle Error* (MAE-L2) as the Euclidean distance of the stacked (ZYX-)Euler angles as well as the *Mean Per Joint Position Error* (MPJPE)

[19] which is calculated using the human’s skeleton forward kinematic. Those are the standard evaluation metrics in deterministic motion prediction [22, 32, 34, 35, 39]. To better understand the influence of the learned latent multimodality we apply an *Best-of-N* evaluation for the MAE-L2 and MPJPE metric. Here we report the value for the motion with the best average metric value over all prediction timesteps originating from the  $N$  modes’ means with the highest probability  $p(z | x)$ .

**Deterministic Baselines.** We evaluate against the following deterministic approaches: (1) *Zero Velocity*: All joints keep their current state at prediction time throughout the entire prediction horizon. (2) *GRU sup.* [37]: Simple encoder-decoder structure using GRUs for variable history and prediction horizon and exponential maps as data representation. (3) *Quaternet* [39]: Encoder-Decoder architecture using GRUs and quaternion data representation. (4) *HistReplItself* [34]: Transformer [45] encoder and fixed prediction horizon graph convolution decoder. Data is pre-processed using the *Discrete Cosine Transform* (DCT) on the time dimension and the model predicts a residual before the output is transformed back using the inverse DCT. For the H3.6M dataset we state the reported values of (2) - (3) and re-run the evaluation of (4) as they originally did not account for  $2\pi$  angle discontinuity. For the AMASS dataset we re-train (4) *HistReplItself* to match our test split. We were not able to compare to some other methods for a lack of open source code (*AGED* [16]) or their computational complexity (*DMGNN* [32] - 62 Million parameter)

**Evaluation Methodology.** It has become common to benchmark on 8 fixed sequences per action of a single test subject on the H3.6M dataset. This has been shown to be un-representative [39]. Thus, we report results on 8 [32, 34, 37, 39] (see Appendix E) and 256 [34, 39] samples per action on the H3.6M data to be comparable to past methods. For the AMASS dataset, we report results on the official test split, consisting of the *Transitions* and *SSM* dataset. While prior authors [34] have argued that the *Transitions* dataset is not suitable for evaluating prediction algorithms for their change of action within sequences, we argue that such behavior can happen in real-world applications. We subsample the H3.6M dataset to 25 HZ and the AMASS dataset to 20 HZ as most of the included datasets have been recorded with a framerate divisible by 20 but not by 25. For the H3.6M dataset, we report metric values previously published on both 8 and 256 samples per action. As the AMASS dataset has been released recently, there are not many published results, yet. Thus, we retrain the current best state-of-the-art algorithm *HistReplItself* and re-train it on the official test split. We train the model on two seconds of history and predict one second into the future.

**Results.** First, we evaluate our approach on common single sample metrics against fully deterministic approaches. Tab. 3 summarizes the results on the H3.6M dataset. Even though we don’t explicitly optimize for a deterministic output, our Weighted-Mean output outperforms

milliseconds	MAE (L2)							
	80	160	320	400	560	720	880	1000
Zero Vel.	0.40	0.70	1.11	1.25	1.46	1.63	1.76	1.84
GRU sup. [37]	0.43	0.74	1.15	1.30	-	-	-	-
Quarternet [39]	0.37	0.62	1.00	1.14	-	-	-	-
HistReptItself [34]	<b>0.28</b>	0.52	0.88	1.02	1.23	<b>1.40</b>	1.55	1.64
Ours W-Mean	<b>0.28</b>	<b>0.51</b>	<b>0.87</b>	<b>1.01</b>	<b>1.22</b>	<b>1.40</b>	<b>1.54</b>	<b>1.63</b>
Ours ML-Mode	0.28	0.51	0.88	1.02	1.24	1.42	1.58	1.67
Ours Bo3-Modes	0.28	0.50	0.85	0.97	1.16	1.31	1.45	1.54
Ours Bo5-Modes	0.28	0.51	0.84	0.96	1.13	1.28	1.42	1.51

Table 3. Average angle error on 256 samples per action on the H3.6M test dataset. A break down by actions and the results on the MPJPE metric can be found in Appendix E.

milliseconds	MAE (L2)					
	100	200	400	600	800	1000
Zero Vel.	0.73	1.20	1.60	1.73	1.76	1.76
HistReptItself [34]	0.45	0.78	1.06	<b>1.17</b>	<b>1.27</b>	<b>1.33</b>
Ours W-Mean	<b>0.42</b>	<b>0.76</b>	<b>1.05</b>	1.19	<b>1.27</b>	<b>1.33</b>
Ours ML-Mode	0.42	0.76	1.08	1.22	1.31	1.38
Ours Bo3-Modes	0.42	0.74	1.01	1.12	1.20	1.28
Ours Bo5-Modes	0.42	0.74	0.99	1.09	1.17	1.27

Table 4. Average angle error on 10,000 samples from the AMASS test set. The MPJPE metric can be found in Appendix E.

all other state-of-the-art algorithms.

We want to point out that we introduced the W-Mean output configuration solely for these metrics commonly used in deterministic evaluation. This allows us to point to the shortcomings of both, deterministic algorithms and their corresponding evaluation metrics: They produce motions which represent the average of all likely motions given the motion history. This average motion, however, may represent a unlikely or even infeasible motion. This (unintentional) behavior is followed by our W-Mean output configuration. Thus, we want to emphasize that while we outperform other algorithms on specific metrics we advise against using the W-Mean output configuration for actual applications.

The lower rows of Tab. 3 and Tab. 4 supports that our approach captures multimodality by committing to a specific motion per mode; thereby attributing appropriate probability mass to less likely motions. As such, the most likely deterministic mode (ML-Mode) commits to the mode which is best explained by the data. However, on average it accumulates a higher error compared to W-Mean as it is expected to represent a “wrong“ motion with probability  $p = 1 - \max_i(\pi_i)$  (see Sec. 5). Looking at the set of likely deterministic mode outputs (BoN in Tab. 3 and Tab. 4), it becomes clear that one of the motion modes performs exceptionally better than the mean output of deterministic regressors. This behavior is further visualized for a single example in Sec. 6.3.

Notably, *Motron* can capture multimodality and reason probabilistically about humans’ future motion while being computationally more efficient than a deterministic regressor. With 1.7 Million parameters we need **half** the computational power than *HistReptItself* (3.4M parameters) and are significantly more efficient compared to the current state-of-the-art algorithm *DLow* with 7.3 Million parameters. Other

milliseconds	NLL			MAE (L2)	
	400	1000	$\sum$	400	1000
$ Z  = 1$	-160.77	-106.10	-4032.58	1.05	1.68
$ Z  = 2$	-173.21	-117.20	-4320.73	1.02	1.63
$ Z  = 3$	-176.25	-121.86	-4405.46	1.02	1.65
$ Z  = 4$	-176.74	<b>-122.03</b>	-4418.98	<b>1.01</b>	<b>1.63</b>
$ Z  = 5$	<b>-177.01</b>	-122.02	<b>-4432.40</b>	<b>1.01</b>	<b>1.63</b>
$ Z  = 6$	-174.50	-117.70	-4340.94	1.01	1.64

Table 5. Negative Log Likelihood (NLL) and MAE (L2) performance using different number of latent modes on H3.6M dataset.

milliseconds	NLL			MAE (L2)	
	400	1000	$\sum$	400	1000
No Typed Graph	-170.28	-112.35	-4264.17	1.07	1.73
One-Hot	-174.78	-119.33	-4372.70	1.04	1.67
Gaussian Mixture Model	-158.56	-102.24	-3879.12	1.06	1.69
Bingham	-162.58	-107.52	-3983.10	1.07	1.67
Latent Grad. Flow	-174.68	-119.99	-4374.77	1.02	1.64
Full	<b>-177.01</b>	<b>-122.02</b>	<b>-4432.40</b>	<b>1.01</b>	<b>1.63</b>

Table 6. Negative Log Likelihood (NLL) and MAE (L2) performance on ablated model structures on H3.6M dataset.

graph based models, such as [32], even use 62 Million parameters.

## 6.2.1 Ablation Study

In this section, we will show the influence of our contributions on the model’s performance as well as justify our design choices quantitatively.

**Number of latent modes.** We ablate the number of latent discrete states which manifest as motion modes in the model’s output (Tab. 5). Four and five modes show the best performance. We use five modes for our approach to give the model more expressiveness when necessary.

**Influence of contributions.** To show the influence of our contributions on the model’s performance we ablate them individually in Tab. 6. We first remove the *Typed Graph* weight sharing scheme and subsequently replace it with One-Hot encoded type information which can recover some performance. Next, we replace the Concentrated Gaussian distribution in SO(3) with a standard Multivariate Normal (Gaussian) Mixture Model (GMM) and subsequently with a Bingham distribution. Unlike our  $\mathcal{N}_{SO(3)}$ , the MVN is not designed to handle rotations and their special characteristics. It, therefore, has worse results in all metrics. The Bingham distribution, in contrast, is designed for rotations but does not support the composition of rotations. Thus, we can not use differential quaternions as intermediate output making the learning task more complex. Also, samples from a Bingham can only be approximated using computationally and memory expensive algorithms (e.g. Metropolis-Hasting). Finally, we enable gradient flow through the latent variable (see Appendix A and Sec. 5), which has a minor negative impact.

## 6.3. Qualitative Results

Fig. 4 shows the capability of our method to capture the multimodal nature of human motions. Displayed is an exemplary motion where the human lands from a jump and

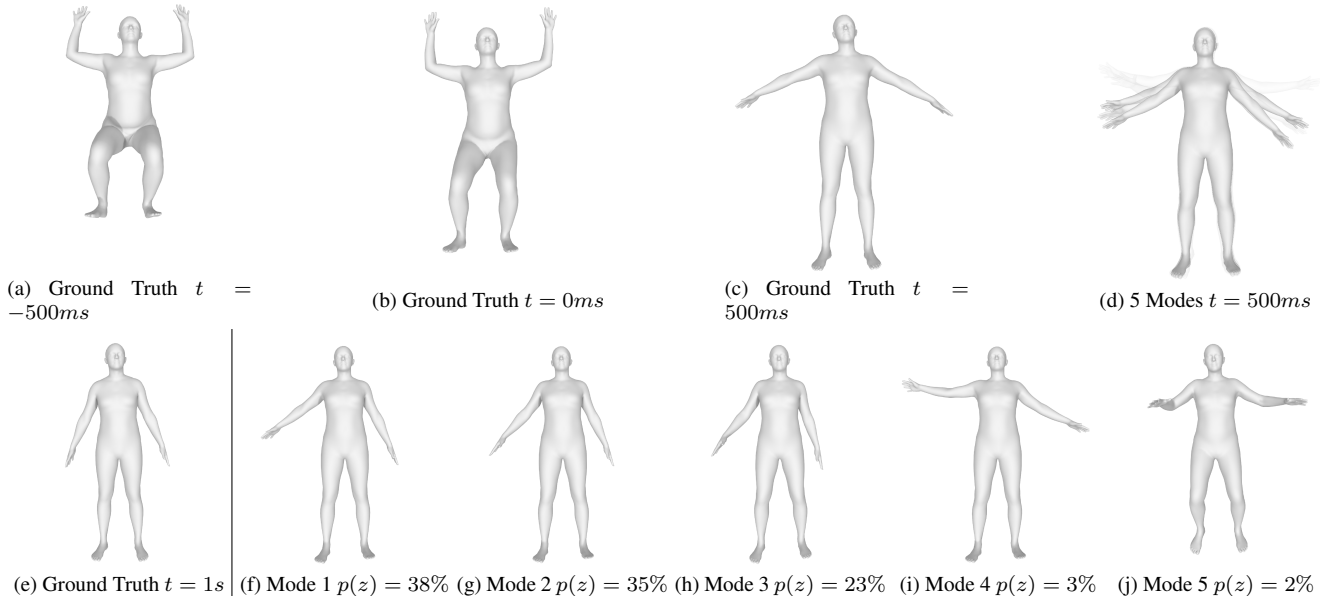


Figure 4. Qualitative visualization of the prediction distribution on a single sample from the AMASS dataset. The human lands from a jump and pulls both arms downwards. (a)-(c), (e) Ground Truth poses. (d) 5 modes of our prediction distribution. Each mode is weighted by its probability where opacity indicates high confidence in a particular mode. (f)-(j) Mean of each of the five output modes at  $t = 1s$ .

rapidly pulls his arms down. In the beginning  $t = 500ms$ , the different latent modes capture different possible speeds of the downwards arm movement. While the most likely mode anticipates a slower downwards movement than performed, the second most likely mode captures the true motion closely. Further, less likely modes capture even faster motions as well as movements where the arms are pulled more in front of the body. Notably, reasonably small uncertainty is presented by the model for other joints. Towards the end  $t = 1000ms$ , the expressiveness and multimodality of the modes can be experienced as, for example, Mode 5 captures the possibility of a consecutive second jump.

Another important quality for robotic applications is the ability to work with imperfect data. To simulate occlusions during training we apply *Node Dropout*. For the occluded nodes, we set a random number of continuous states leading to  $t = 0$  to the neutral quaternion. The unique capabilities of our model here are shown in Fig. 5. In this instance, we artificially occlude all joint’s data of the left leg. This leads to high variance but reasonable sampled predictions during early timesteps. More importantly, the model can understand and output its uncertainty: The closed form standard deviation of the parametric  $\mathcal{N}_{SO(3)}^\pi$  output distribution is adequately higher compared to the distribution with perfect data. For increasing prediction time, the model uses the influence between nodes learned in the *Typed Graph* layers to produce reasonable motions even for the occluded nodes and adjusts its relative confidence reasonably.

## 7. Conclusion

In this work, we present *Motron*, a generative human motion forecasting approach which uniquely provides the information plethora of a generative approach and the accu-

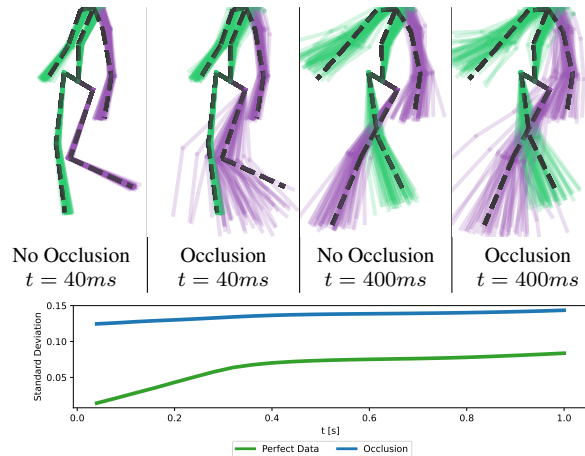


Figure 5. Handling of imperfect data. All joints of the left leg are artificially occluded. *Top*: Visualization of prediction samples with and without occlusion. *Bottom*: Mean standard deviation of parametric output distribution of left hip and knee. The occluded data is addressed by the model adjusting its own uncertainty.

racy of a deterministic model. Its predictions respect kinematic constraints, all while producing full parametric motion distributions, which can be especially useful in downstream robotic applications. It achieves state-of-the-art prediction performance in a variety of metrics on standard and new real-world human motion datasets. Further, to the best of the authors’ knowledge, it is the first method that demonstrates its ability to deal with occluded data while reasoning about its own uncertainty.

**Limitations.** The approach is jet limited by the upstream data provider. While the motion capture system utilized to record the datasets used here provides the required accuracy



to calculate the joint rotations via inverse kinematics, the authors anticipate this being a challenge when relying on vision-based algorithms for human poses detection.

**Future Directions** include incorporating *Motron*'s human behavior predictions in downstream robotic planning, decision making, and control frameworks, as well as exploring options to tightly couple upstream vision algorithms.

## References

- [1] Sadegh Aliakbarian, Fatemeh Sadat Saleh, Lars Petersson, Stephen Gould, and Mathieu Salzmann. Contextually Plausible and Diverse 3D Human Motion Prediction. In *Proceedings of the IEEE/CVF International Conference on Computer Vision*, 12 2021. 2, 5
- [2] Timothy D Barfoot. *State Estimation for Robotics*. Cambridge University Press, 2021. 2, 3
- [3] Emad Barsoum, John Kender, and Zicheng Liu. HP-GAN: Probabilistic 3D human motion prediction via GAN. In *IEEE Conference on computer vision and pattern recognition workshops*, 11 2017. 2
- [4] Apratim Bhattacharyya, Bernt Schiele, and Mario Fritz. Accurate and Diverse Sampling of Sequences based on a "Best of Many" Sample Objective. In *IEEE Conference on Computer Vision and Pattern Recognition*, 6 2018. 5, 6
- [5] Christopher Bingham. An antipodally symmetric distribution on the sphere. *The Annals of Statistics*, pages 1201–1225, 1974. 2
- [6] Eli Bingham, Jonathan P. Chen, Martin Jankowiak, Fritz Obermeyer, Neeraj Pradhan, Theofanis Karaletsos, Rohit Singh, Paul Szerlip, Paul Horsfall, and Noah D. Goodman. Pyro: Deep Universal Probabilistic Programming. *Journal of Machine Learning Research*, 10 2018. 2
- [7] Christopher M Bishop. Mixture Density Networks. Technical report, 1994. 2
- [8] Nat Dilokthanakul, Pedro A. M. Mediano, Marta Garnelo, Matthew C. H. Lee, Hugh Salimbeni, Kai Arulkumaran, and Murray Shanahan. Deep Unsupervised Clustering with Gaussian Mixture Variational Autoencoders. In *International Conference on Learning Representations*, 11 2017. 5, 6
- [9] Ronald Fisher. Dispersion on a Sphere. *Proceedings of the Royal Society of London. Series A*, 217(1130):295–305, 1953. 2
- [10] Katerina Fragkiadaki, Sergey Levine, Panna Felsen, and Jitendra Malik. Recurrent Network Models for Human Dynamics. In *Proceedings of the IEEE International Conference on Computer Vision*, 8 2015. 2
- [11] Partha Ghosh, Jie Song, Emre Aksan, and Otmar Hilliges. Learning Human Motion Models for Long-term Predictions. In *International Conference on 3D Vision*, 4 2017. 2
- [12] Igor Gilitschenski, Gerhard Kurz, Simon J Julier, and Uwe D Hanebeck. Efficient Bingham Filtering Based on Saddlepoint Approximations. In *International Conference on Multisensor Fusion and Information Integration for Intelligent Systems (MFI)*, 2014. 2
- [13] Igor Gilitschenski, Roshni Sahoo, Wilko Schwarting, Alexander Amini, Sertac Karaman, and Daniela Rus. Deep Orientation Uncertainty Learning Based on a Bingham Loss. In *International Conference on Learning Representations (ICLR)*, 2020. 2
- [14] Jared Glover. *The Quaternion Bingham Distribution, Detection, and Dynamic Manipulation*. PhD thesis, Massachusetts Institute of Technology, Cambridge, 2014. 2
- [15] F Sebastian Grassia. Practical Parameterization of Rotations Using the Exponential Map. Technical Report 3, 1998. 3
- [16] Liang-Yan Gui, Yu-Xiong Wang, Xiaodan Liang, and José M F Moura. Adversarial Geometry-Aware Human Motion Prediction. In *Proceedings of the European Conference on Computer Vision (ECCV)*, pages 786–803, 2018. 2, 6
- [17] Swaminathan Gurumurthy, Ravi Kiran Sarvadevabhatla, and Venkatesh Babu Radhakrishnan. DeLiGAN: Generative Adversarial Networks for Diverse and Limited Data. In *IEEE Conference on Computer Vision and Pattern Recognition*, 6 2017. 2, 5, 6
- [18] Irina Higgins, Loic Matthey, Arka Pal, Christopher Burgess, Xavier Glorot, Matthew Botvinick, Shakir Mohamed, Alexander Lerchner, and Google Deepmind.  $\beta$ -VAE: Learning Basic Visual Concepts with a Constrained Variational Framework. In *International Conference on Learning Representations*, 2016. 4
- [19] Catalin Ionescu, Dragos Papava, Vlad Olaru, and Cristian Sminchisescu. Human3.6M: Large Scale Datasets and Predictive Methods for 3D Human Sensing in Natural Environments. Technical report, 2014. 2, 5, 6
- [20] Boris Ivanovic and Marco Pavone. The Trajectron: Probabilistic Multi-Agent Trajectory Modeling With Dynamic Spatiotemporal Graphs. In *IEEE/CVF International Conference on Computer Vision*, 10 2019. 5
- [21] Boris Ivanovic, Edward Schmerling, Karen Leung, and Marco Pavone. Generative Modeling of Multimodal Multi-Human Behavior. In *IEEE/RSJ International Conference on Intelligent Robots and Systems (IROS)*, 2018. 4
- [22] Ashesh Jain, Amir R. Zamir, Silvio Savarese, and Ashutosh Saxena. Structural-RNN: Deep Learning on Spatio-Temporal Graphs. 11 2015. 2, 6
- [23] Eric Jang, Shixiang Gu, and Ben Poole. Categorical Reparameterization with Gumbel-Softmax. In *International Conference on Learning Representations*, 11 2017. 4
- [24] Diederik P Kingma and Max Welling. Auto-Encoding Variational Bayes. *arXiv preprint arXiv:1312.6114*, 12 2013. 4
- [25] Thomas N. Kipf and Max Welling. Semi-Supervised Classification with Graph Convolutional Networks. In *International Conference on Learning Representations*, 9 2017. 3
- [26] Vineet Kosaraju, Amir Sadeghian, Roberto Martín-Martín, Ian Reid, S. Hamid Rezaatofighi, and Silvio Savarese. Social-BiGAT: Multimodal Trajectory Forecasting using BicycleGAN and Graph Attention Networks. In *Advances in Neural Information Processing Systems*, 7 2019. 2
- [27] Jogendra Nath Kundu, Maharshi Gor, and R. Venkatesh Babu. BiHMP-GAN: Bidirectional 3D Human Motion Prediction GAN. In *AAAI Conference on Artificial Intelligence*, 12 2018. 2
- [28] Gerhard Kurz, Igor Gilitschenski, and Uwe D Hanebeck. Efficient Evaluation of the Probability Density Function of a Wrapped Normal Distribution. Technical report. 2
- [29] Gerhard Kurz, Igor Gilitschenski, Florian Pfaff, Lukas Drude, Uwe Hanebeck, Reinhold Haeb-Umbach, and Roland Siegwart. Statistics and Filtering Using libDirectional. *Journal of Statistical Software Directional*, 89(4):1–31, 2017. 2

- [30] Muriel Lang. *Approximation of probability density functions on the Euclidean group parametrized by dual quaternions*. PhD thesis. [2](#)
- [31] Andreas M Lehmman, Peter V Gehler, and Sebastian Nowozin. Efficient Nonlinear Markov Models for Human Motion. In *Conference on Computer Vision and Pattern Recognition*, 2014. [2](#)
- [32] Maosen Li, Siheng Chen, Yangheng Zhao, Ya Zhang, Yanfeng Wang, and Qi Tian. Dynamic Multiscale Graph Neural Networks for 3D Skeleton-Based Human Motion Prediction. In *The IEEE/CVF Conference on Computer Vision and Pattern Recognition (CVPR)*, 6 2020. [2](#), [3](#), [6](#), [7](#), [14](#)
- [33] Naureen Mahmood, Nima Ghorbani, Nikolaus F Troje, Gerard Pons-Moll, and Michael J Black. AMASS: Archive of Motion Capture as Surface Shapes. In *International Conference on Computer Vision*, pages 5442–5451, 2019. [5](#)
- [34] Wei Mao, Miaomiao Liu, and Mathieu Salzmann. History Repeats Itself: Human Motion Prediction via Motion Attention. In *European Conference on Computer Vision*, 2020. [2](#), [6](#), [7](#), [13](#), [14](#), [15](#)
- [35] Wei Mao, Miaomiao Liu, Mathieu Salzmann, and Hongdong Li. Learning Trajectory Dependencies for Human Motion Prediction. *Proceedings of the IEEE/CVF International Conference on Computer Vision*, 8 2019. [2](#), [3](#), [6](#)
- [36] F. Landis Markley, Yang Cheng, John Crassidis, and Yaakov Oshman. Averaging Quaternions. In *Journal of Guidance, Control, and Dynamics*, 2007. [5](#)
- [37] Julieta Martinez, Michael J Black, and Javier Romero. On human motion prediction using recurrent neural networks. Technical report, 2017. [2](#), [6](#), [7](#), [13](#), [14](#)
- [38] Emanuel Parzen. On Estimation of a Probability Density Function and Mode. *Ann. Math. Statist.*, 33, 1962. [5](#)
- [39] Dario Pavllo, Christoph Feichtenhofer, Michael Auli, and David Grangier. Modeling Human Motion with Quaternion-based Neural Networks. *International Journal of Computer Vision*, 1 2019. [2](#), [3](#), [6](#), [7](#), [11](#), [13](#)
- [40] Vladimir Pavlovic, James M Rehg, and John Maccormick. Learning Switching Linear Models of Human Motion. In *Advances in Neural Information Processing Systems*, 2000. [2](#)
- [41] Valentin Peretroukhin, Matthew Giamou, David M. Rosen, W. Nicholas Greene, Nicholas Roy, and Jonathan Kelly. A Smooth Representation of Belief over  $SO(3)$  for Deep Rotation Learning with Uncertainty. In *Proceedings of Robotics: Science and Systems (RSS)*, 6 2020. [2](#)
- [42] Tim Salzmann, Boris Ivanovic, Punarjay Chakravarty, and Marco Pavone. Trajectron++: Dynamically-Feasible Trajectory Forecasting With Heterogeneous Data. In *European Conference on Computer Vision (ECCV)*, 2020. [2](#), [4](#)
- [43] Yongyi Tang, Lin Ma, Wei Liu, and Wei-Shi Zheng. Long-Term Human Motion Prediction by Modeling Motion Context and Enhancing Motion Dynamics. In *International Joint Conference on Artificial Intelligence*, pages 935–941, 2018. [2](#)
- [44] Yichuan Charlie Tang and Ruslan Salakhutdinov. Multiple Futures Prediction. In *Advances in neural information processing systems*, 11 2019. [2](#)
- [45] Ashish Vaswani, Noam Shazeer, Niki Parmar, Jakob Uszkoreit, Llion Jones, Aidan N. Gomez, Lukasz Kaiser, and Illia Polosukhin. Attention Is All You Need. In *Advances in neural information processing systems*, 6 2017. [2](#), [6](#)
- [46] Petar Veličković, Guillem Cucurull, Arantxa Casanova, Adriana Romero, Pietro Liò, and Yoshua Bengio. Graph Attention Networks. In *International Conference on Learning Representations*, 10 2017. [2](#), [3](#)
- [47] Jacob Walker, Kenneth Marino, Abhinav Gupta, and Martial Hebert. The Pose Knows: Video Forecasting by Generating Pose Futures. In *International Conference on Computer Vision*, 4 2017. [5](#), [6](#)
- [48] Jack M. Wang, David J. Fleet, and Aaron Hertzmann. Gaussian process dynamical models for human motion. *IEEE Transactions on Pattern Analysis and Machine Intelligence*, 30(2):283–298, 2 2008. [2](#)
- [49] Tianlong Wu, Feng Chen, and Yun Wan. Graph Attention LSTM Network: A New Model for Traffic Flow Forecasting. In *Proceedings - 2018 5th International Conference on Information Science and Control Engineering, ICISCE 2018*, pages 241–245. Institute of Electrical and Electronics Engineers Inc., 1 2019. [2](#)
- [50] Xinchen Yan, Akash Rastogi, Ruben Villegas, Kalyan Sunkavalli, Eli Shechtman, Sunil Hadap, Ersin Yumer, and Honglak Lee. MT-VAE: Learning Motion Transformations to Generate Multimodal Human Dynamics. In *European Conference on Computer Vision*, 8 2018. [5](#), [6](#)
- [51] Ye Yuan and Kris Kitani. Diverse Trajectory Forecasting with Determinantal Point Processes. In *International Conference on Learning Representations*, 2020. [2](#), [5](#), [11](#)
- [52] Ye Yuan and Kris Kitani. DLow: Diversifying Latent Flows for Diverse Human Motion Prediction. In *Proceedings of the European Conference on Computer Vision (ECCV)*, 3 2020. [2](#), [5](#), [6](#)
- [53] Yan Zhang, Michael J. Black, and Siyu Tang. We are More than Our Joints: Predicting how 3D Bodies Move. In *Proceedings of the IEEE/CVF Conference on Computer Vision and Pattern Recognition*, 2021. [2](#)
- [54] Jie Zhou, Ganqu Cui, Zhengyan Zhang, Cheng Yang, Zhiyuan Liu, Lifeng Wang, Changcheng Li, and Maosong Sun. Graph Neural Networks: A Review of Methods and Applications. *AI Open*, 1, 2020. [2](#)

## A. Gradient Flow Through Latent Variable

A reparameterization trick (Gumbel-Softmax) is commonly used to approximate the expectation  $\mathbb{E}_{z \sim q_\psi(\cdot|x)}$  by taking  $N$  samples from  $q_\psi(z|x)$ . We however, using the latent distribution in the output representation, exactly compute  $\mathbb{E}_{z \sim q_\psi(\cdot|x)} = \sum_z \log q_\psi(z|x) p_\psi(y|x, z)$ .

Still the gradient resulting from each component’s Log-Likelihood could be backpropagated to update  $\phi$ . Conceptually, we argue that the mixture distribution should not affect the individual component distributions’ log-prob computation. The same applies to the gradients. Practically, letting the gradient flow through the latent variable a marginal negative experimental influence on the performance. Thus, as the implementation difference is a single line, we will leave the choice to the user.

## B. Implementation and Training Details

All model training was performed on a single *Nvidia RTX2080*.

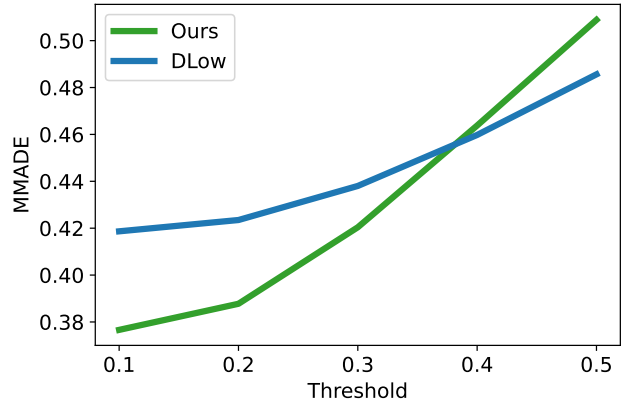
**Deterministic Evaluation.** For the H3.6M dataset, we applied dataset augmentation (according to [39]) where the training samples are mirrored along the human’s vertical. A batch size of 32 and early stopping to select the best model was used. During hyperparameter optimization, we used subject 6 for validation purposes. For the final model, subject 6 was added to the training data, but we kept the same early stopping iteration which showed the best performance during validation. All test evaluations were performed on the full 32-joint skeleton of subject 5. For the AMASS dataset we use 5% of the training data samples as validation data. Again, we use early stopping based on the validation results. The batch size for AMASS is 128. All evaluations were performed on the full 22-joint skeleton.

**Generative Evaluation.** We use the same hyperparameters for the H3.6M dataset as in the deterministic evaluation. However, according to previous works, we only evaluate on the positions of a 16-joints skeleton where subject 9 and 11 serve as test subjects. To stabilize the GRU for the long prediction horizon (100 steps) we use a form of curriculum learning; increasing the prediction horizon from a small value to the target in early iterations.

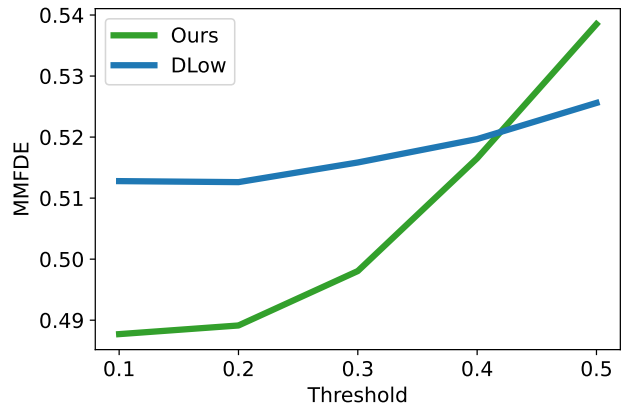
For both model types we found it beneficial to randomly shrink the prediction horizon at every training iteration.

## C. Multimodal Metrics

In [51] the authors propose two multimodal evaluation metrics where motions are combined based on ”similar context” and evaluate the mean performance on all futures of the combined motions. Their measure of similarity is solely based on the distance of motions at a single timestep  $t = 0$ . Motions are combined for evaluation using a threshold on that distance. While this threshold is arbitrarily set to 0.5 in [51], we use a range of different thresholds in our evaluation. The results can be seen in Fig. 6. While we outperform *DLow* for lower thresholds we have lower numerical results for higher thresholds. However, looking at a concrete example Fig. 7 we see that for high thresholds motions with entirely uncorrelated futures (and history) are combined for evaluation. Thus, the worse numerical results for (too) high thresholds are expected; even encouraged here.



(a) MMADE for different thresholds



(b) MMFDE for different thresholds

Figure 6. Result for multimodal metrics proposed in [51] for different thresholds. For larger thresholds, where possibly uncorrelated motions are evaluated together, *DLow* achieves better numerical values as their approaches over-diversifies their produced motions.

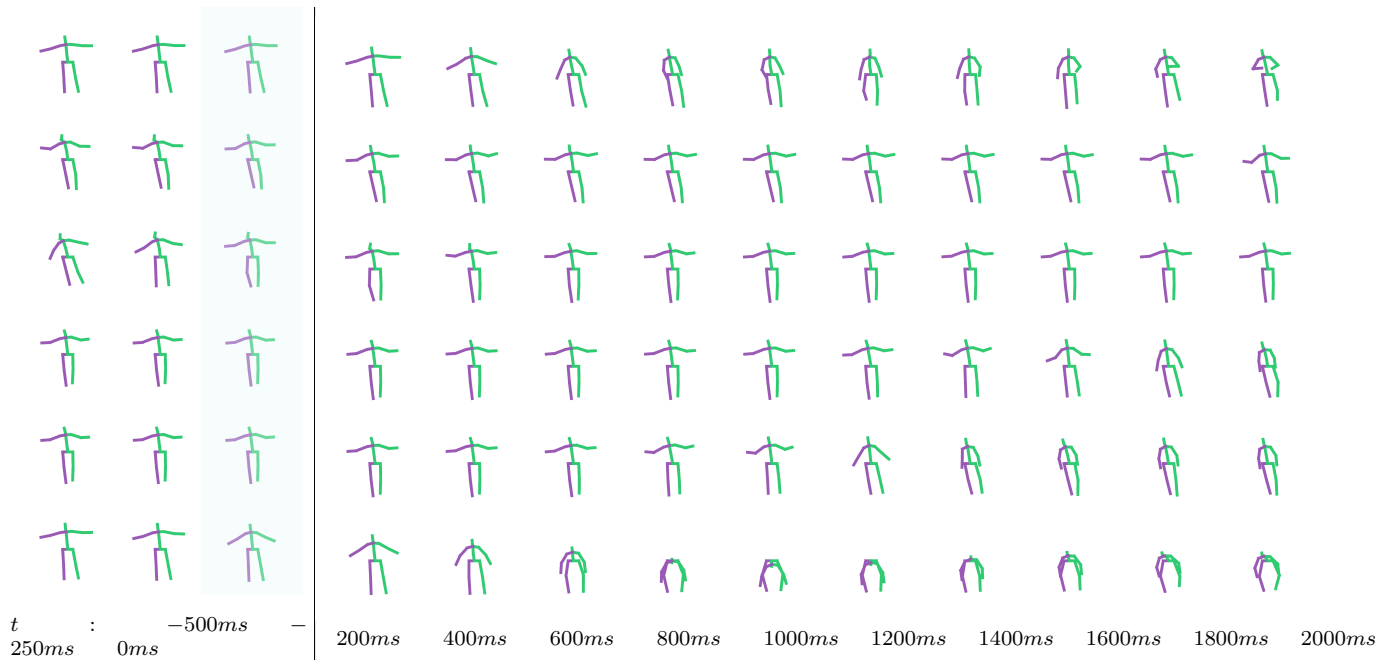


Figure 7. Example of 6 motions which are combined for the multimodal evaluation. At  $t = 0$  (highlighted) all motions seem to be similar. However, they greatly differ in history and future. Thus, we do not expect, and do not want, our model to give accurate output for all futures when only the history of the first motion is used as input.

## D. Bone Deformation

Some algorithms directly predict joint positions instead of joint configurations (angles). This shows advantages on metrics calculated on joint positions (e.g. MPJPE). However, as Fig. 8 outlines they produce physically unfeasible motions as the rigid bone structure is deformed.

## E. Further Deterministic Results

We present additional results for the deterministic evaluation. In Tab. 7 the results are split up by individual actions for 256 samples and for 8 samples in Tab. 8. We also present the MPJPE metric which is calculated on the joint's position using forward kinematic on angle outputs (Tab. 9 and Tab. 10).

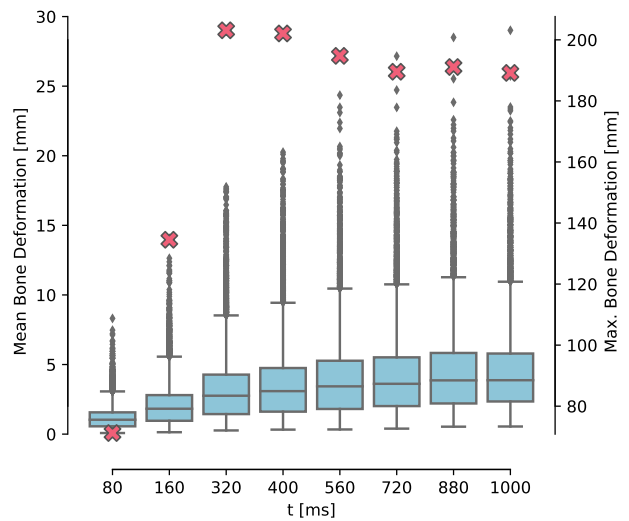


Figure 8. Exemplary bone deformation of a method directly predicting 3D joint positions. With increasing prediction time the deformation increases with outliers reaching deformations of over 20cm. Boxplots: Mean bone deformation over all bones in the skeleton. Red Crosses: Maximum bone deformation over all bones. Analysis performed on 10000 samples.

Average										Walking										Eating									
milliseconds	80	160	320	400	560	720	880	1000		80	160	320	400	560	720	880	1000		80	160	320	400	560	720	880	1000			
Zero Vel.	0.40	0.70	1.11	1.25	1.46	1.63	1.76	1.84		0.43	0.78	1.23	1.34	1.50	1.56	1.58	1.55		0.28	0.53	0.89	1.03	1.18	1.33	1.44	1.49			
GRU sup. [37]	0.43	0.74	1.15	1.30	-	-	-	-		0.34	0.60	0.91	0.98	-	-	-	-		0.30	0.57	0.87	0.98	-	-	-	-			
Quarternet [39]	0.37	0.62	1.00	1.14	-	-	-	-		0.28	0.49	0.76	0.83	-	-	-	-		0.22	0.47	0.76	0.88	-	-	-	-			
HistReptItself [34]	0.28	0.52	0.88	1.02	1.23	1.40	1.55	1.64		0.24	0.43	0.66	0.71	0.84	0.91	0.99	1.03		0.18	0.37	0.67	0.79	0.95	1.11	1.23	1.30			
Ours W-Mean	0.28	0.51	0.87	1.01	1.22	1.40	1.54	1.63		0.23	0.43	0.68	0.74	0.88	0.94	1.03	1.08		0.20	0.41	0.79	0.90	1.06	1.23	1.38	1.45			
Ours ML-Mode	0.28	0.51	0.88	1.02	1.24	1.42	1.58	1.67		0.23	0.43	0.68	0.73	0.88	0.94	1.04	1.10		0.20	0.41	0.79	0.91	1.06	1.23	1.39	1.47			
Smoking										Discussion										Directions									
milliseconds	80	160	320	400	560	720	880	1000		80	160	320	400	560	720	880	1000		80	160	320	400	560	720	880	1000			
Zero Vel.	0.30	0.53	0.88	1.03	1.23	1.38	1.52	1.62		0.46	0.80	1.22	1.36	1.62	1.74	1.83	1.90		0.30	0.54	0.92	1.08	1.24	1.35	1.48	1.54			
GRU sup. [37]	0.35	0.69	1.14	1.29	-	-	-	-		0.54	0.85	1.30	1.44	-	-	-	-		0.32	0.58	0.97	1.14	-	-	-	-			
Quarternet [39]	0.28	0.47	0.79	0.91	-	-	-	-		0.38	0.74	1.20	1.37	-	-	-	-		0.24	0.46	0.84	1.01	-	-	-	-			
HistReptItself [34]	0.21	0.38	0.65	0.79	0.99	1.15	1.30	1.42		0.31	0.61	1.02	1.17	1.44	1.57	1.68	1.76		0.19	0.38	0.74	0.90	1.08	1.22	1.35	1.42			
Ours W-Mean	0.21	0.38	0.65	0.80	1.02	1.32	1.34	1.44		0.36	0.63	1.02	1.16	1.41	1.54	1.63	1.70		0.19	0.38	0.75	0.94	1.13	1.26	1.38	1.46			
Ours ML-Mode	0.21	0.38	0.65	0.80	1.03	1.22	1.36	1.47		0.35	0.63	1.02	1.18	1.44	1.58	1.68	1.75		0.19	0.38	0.76	0.95	1.15	1.28	1.40	1.48			
Greeting										Phoning										Posing									
milliseconds	80	160	320	400	560	720	880	1000		80	160	320	400	560	720	880	1000		80	160	320	400	560	720	880	1000			
Zero Vel.	0.54	0.91	1.41	1.59	1.81	2.01	2.16	2.23		0.39	0.69	1.14	1.28	1.48	1.70	1.85	1.91		0.40	0.74	1.20	1.40	1.72	2.00	2.29	2.44			
GRU sup. [37]	0.64	0.99	1.40	1.54	-	-	-	-		0.42	0.70	1.11	1.27	-	-	-	-		0.46	0.83	1.33	1.52	-	-	-	-			
Quarternet [39]	0.61	0.93	1.34	1.51	-	-	-	-		0.36	0.61	0.98	1.14	-	-	-	-		0.38	0.71	1.20	1.39	-	-	-	-			
HistReptItself [34]	0.39	0.71	1.17	1.35	1.60	1.78	1.93	1.99		0.29	0.52	0.91	1.05	1.24	1.47	1.63	1.72		0.27	0.55	1.00	1.21	1.54	1.80	2.10	2.24			
Ours W-Mean	0.40	0.68	1.14	1.31	1.51	1.70	1.84	1.90		0.28	0.51	0.84	0.98	1.19	1.41	1.58	1.66		0.24	0.50	0.93	1.12	1.42	1.71	1.96	2.10			
Ours ML-Mode	0.40	0.69	1.14	1.32	1.53	1.75	1.92	1.98		0.28	0.51	0.85	1.00	1.21	1.45	1.61	1.70		0.24	0.50	0.94	1.13	1.45	1.76	2.03	2.19			
Purchases										Sitting										Sitting Down									
milliseconds	80	160	320	400	560	720	880	1000		80	160	320	400	560	720	880	1000		80	160	320	400	560	720	880	1000			
Zero Vel.	0.57	0.96	1.36	1.44	1.64	1.79	1.94	2.01		0.33	0.60	1.01	1.16	1.41	1.67	1.87	1.98		0.50	0.84	1.30	1.48	1.99	2.21	2.31				
GRU sup. [37]	0.57	0.95	1.33	1.43	-	-	-	-		0.41	0.75	1.22	1.41	-	-	-	-		0.59	1.00	1.62	1.87	-	-	-	-			
Quarternet [39]	0.54	0.92	1.36	1.47	-	-	-	-		0.34	0.59	1.00	1.15	-	-	-	-		0.47	0.81	1.31	1.50	-	-	-	-			
HistReptItself [34]	0.43	0.78	1.21	1.31	1.47	1.62	1.74	1.81		0.25	0.49	0.91	1.06	1.33	1.59	1.78	1.88		0.41	0.72	1.17	1.36	1.66	1.88	2.11	2.20			
Ours W-Mean	0.44	0.75	1.18	1.28	1.48	1.69	1.77	1.86		0.23	0.45	0.85	1.01	1.28	1.53	1.70	1.81		0.41	0.72	1.17	1.36	1.68	1.90	2.12	2.22			
Ours ML-Mode	0.44	0.75	1.19	1.29	1.52	1.74	1.82	1.91		0.23	0.46	0.87	1.02	1.30	1.56	1.74	1.84		0.41	0.73	1.18	1.37	1.69	1.91	2.14	2.24			
Taking Photo										Waiting										Walk Dog									
milliseconds	80	160	320	400	560	720	880	1000		80	160	320	400	560	720	880	1000		80	160	320	400	560	720	880	1000			
Zero Vel.	0.26	0.44	0.73	0.84	1.05	1.20	1.33	1.45		0.37	0.64	1.10	1.27	1.50	1.67	1.91	1.92		0.53	0.85	1.20	1.31	1.46	1.63	1.73	1.78			
GRU sup. [37]	0.30	0.52	0.88	1.02	-	-	-	-		0.41	0.68	1.20	1.37	-	-	-	-		0.52	0.84	1.21	1.32	-	-	-	-			
Quarternet [39]	0.23	0.39	0.69	0.81	-	-	-	-		0.32	0.54	1.00	1.15	-	-	-	-		0.48	0.78	1.12	1.21	-	-	-	-			
HistReptItself [34]	0.19	0.34	0.60	0.72	0.92	1.07	1.21	1.33		0.25	0.46	0.88	1.05	1.28	1.47	1.63	1.75		0.41	0.68	1.01	1.12	1.30	1.45	1.54	1.63			
Ours W-Mean	0.20	0.33	0.60	0.72	0.91	1.10	1.25	1.36		0.23	0.44	0.83	1.00	1.23	1.42	1.58	1.69		0.41	0.69	1.05	1.16	1.30	1.48	1.59	1.68			
Ours ML-Mode	0.20	0.33	0.60	0.72	0.92	1.10	1.26	1.38		0.24	0.44	0.84	1.00	1.23	1.42	1.58	1.70		0.41	0.69	1.07	1.17	1.32	1.50	1.63	1.72			
Walk Together																													
milliseconds	80	160	320	400	560	720	880	1000																					
Zero Vel.	0.37	0.66	1.02	1.15	1.32	1.39	1.41	1.43																					
GRU sup. [37]	0.35	0.57	0.83	0.94	-	-	-	-																					
Quarternet [39]	0.28	0.45	0.69	0.79	-	-	-	-																					
HistReptItself [34]	0.21	0.38	0.62	0.71	0.86	0.94	1.00	1.04																					
Ours W-Mean	0.20	0.36	0.59	0.68	0.83	0.92	1.01	1.06																					
Ours ML-Mode	0.20	0.36	0.59	0.68	0.84	0.94	1.04	1.09																					

Table 7. Angle error on 256 samples per action on the H3.6M test dataset.

milliseconds	Average								Walking								Eating							
	80	160	320	400	560	720	880	1000	80	160	320	400	560	720	880	1000	80	160	320	400	560	720	880	1000
Zero Vel.	0.40	0.71	1.07	1.20	1.42	1.57	1.75	1.85	0.39	0.68	0.99	1.15	1.35	1.37	1.34	1.32	0.27	0.48	0.73	0.86	1.04	1.10	1.27	1.38
GRU sup. [37]	0.40	0.69	1.04	1.18	-	-	-	-	0.27	0.46	0.67	0.75	0.93	-	-	1.03	0.23	0.37	0.59	0.73	0.95	-	-	1.08
DMGNN [32]	0.27	0.52	0.83	0.95	-	-	-	-	0.18	0.31	0.49	0.58	0.66	-	-	0.75	0.17	0.30	0.49	0.59	0.74	-	-	1.14
HistReptItself [34]	0.27	0.52	0.82	0.93	1.14	1.28	1.48	1.59	0.18	0.30	0.46	0.51	0.59	0.62	0.61	0.64	0.16	0.29	0.49	0.60	0.74	0.81	1.01	1.11
Ours W-Mean	0.26	0.48	0.81	0.93	1.12	1.28	1.46	1.56	0.18	0.31	0.51	0.55	0.61	0.65	0.64	0.66	0.16	0.29	0.49	0.61	0.72	0.77	0.96	1.07
Ours ML-Mode	0.26	0.48	0.82	0.95	1.15	1.32	1.50	1.60	0.18	0.31	0.51	0.56	0.61	0.65	0.64	0.67	0.16	0.30	0.50	0.62	0.73	0.78	0.97	1.08
milliseconds	Smoking								Discussion								Directions							
	80	160	320	400	560	720	880	1000	80	160	320	400	560	720	880	1000	80	160	320	400	560	720	880	1000
Zero Vel.	0.26	0.48	0.97	0.95	1.02	1.14	1.47	1.69	0.31	0.67	0.94	1.04	1.41	1.71	1.86	1.96	0.39	0.59	0.79	0.89	1.02	1.22	1.47	1.50
GRU sup. [37]	0.32	0.59	1.01	1.10	1.25	-	-	1.50	0.30	0.67	0.98	1.06	1.43	-	-	1.69	0.41	0.64	0.80	0.92	-	-	-	-
DMGNN [32]	0.21	0.39	0.81	0.77	0.83	-	-	1.52	0.26	0.65	0.92	0.99	1.33	-	-	1.45	0.25	0.44	0.65	0.71	-	-	-	-
HistReptItself [34]	0.22	0.42	0.86	0.80	0.86	1.00	1.34	1.58	0.20	0.52	0.78	0.87	1.30	1.54	1.66	1.72	0.25	0.43	0.60	0.69	0.81	1.03	1.25	1.29
Ours W-Mean	0.21	0.42	0.79	0.89	0.96	1.02	1.33	1.48	0.21	0.56	0.80	0.90	1.23	1.51	1.57	1.53	0.29	0.38	0.63	0.72	0.87	1.08	1.29	1.34
Ours ML-Mode	0.21	0.43	0.82	0.93	1.01	1.09	1.40	1.56	0.21	0.56	0.81	0.92	1.26	1.54	1.61	1.58	0.29	0.39	0.67	0.77	0.97	1.16	1.37	1.42
milliseconds	Greeting								Phoning								Posing							
	80	160	320	400	560	720	880	1000	80	160	320	400	560	720	880	1000	80	160	320	400	560	720	880	1000
Zero Vel.	0.54	0.89	1.30	1.49	1.79	1.77	1.85	1.80	0.64	1.21	1.57	1.70	1.81	1.94	2.05	2.04	0.28	0.57	1.13	1.37	1.81	2.23	2.58	2.78
GRU sup. [37]	0.57	0.82	1.45	1.60	-	-	-	-	0.59	1.06	1.45	1.60	-	-	-	-	0.45	0.85	1.34	1.56	-	-	-	-
DMGNN [32]	0.36	0.61	0.94	1.12	-	-	-	-	0.52	0.97	1.29	1.43	-	-	-	-	0.20	0.46	1.06	1.34	-	-	-	-
HistReptItself [34]	0.35	0.60	0.95	1.14	1.48	1.47	1.61	1.57	0.53	1.01	1.22	1.29	1.42	1.55	1.68	1.68	0.19	0.46	1.09	1.35	1.59	1.83	2.14	2.34
Ours W-Mean	0.35	0.58	0.87	1.03	1.29	1.34	1.53	1.54	0.41	0.62	1.12	1.19	1.36	1.39	1.53	1.69	0.19	0.48	1.03	1.25	1.55	1.96	2.22	2.39
Ours ML-Mode	0.35	0.59	0.87	1.02	1.28	1.31	1.50	1.53	0.42	0.63	1.16	1.24	1.48	1.54	1.66	1.81	0.19	0.48	1.03	1.26	1.66	2.12	2.40	2.58
milliseconds	Purchases								Sitting								Sitting Down							
	80	160	320	400	560	720	880	1000	80	160	320	400	560	720	880	1000	80	160	320	400	560	720	880	1000
Zero Vel.	0.62	0.88	1.19	1.27	1.64	1.62	2.09	2.45	0.40	0.63	1.02	1.18	1.26	1.36	1.57	1.63	0.39	0.74	1.07	1.19	1.36	1.57	1.70	1.80
GRU sup. [37]	0.58	0.79	1.08	1.15	-	-	-	-	0.41	0.68	1.12	1.33	-	-	-	-	0.47	0.88	1.37	1.54	-	-	-	-
DMGNN [32]	0.41	0.61	1.05	1.14	-	-	-	-	0.26	0.42	0.76	0.97	-	-	-	-	0.32	0.65	0.93	1.05	-	-	-	-
HistReptItself [34]	0.42	0.65	1.00	1.07	1.43	1.53	1.94	2.24	0.29	0.47	0.83	1.01	1.16	1.29	1.50	1.55	0.30	0.63	0.92	1.04	1.18	1.42	1.55	1.69
Ours W-Mean	0.41	0.64	1.06	1.14	1.42	1.66	2.00	2.28	0.26	0.44	0.79	0.99	1.12	1.28	1.52	1.58	0.29	0.60	0.93	1.08	1.30	1.51	1.64	1.78
Ours ML-Mode	0.42	0.64	1.07	1.17	1.44	1.73	2.08	2.33	0.26	0.43	0.78	0.98	1.09	1.25	1.49	1.55	0.29	0.60	0.94	1.10	1.30	1.50	1.63	1.76
milliseconds	Taking Photo								Waiting								Walk Dog							
	80	160	320	400	560	720	880	1000	80	160	320	400	560	720	880	1000	80	160	320	400	560	720	880	1000
Zero Vel.	0.25	0.51	0.79	0.92	1.03	1.13	1.22	1.27	0.34	0.67	1.22	1.47	1.89	2.27	2.57	2.63	0.60	0.98	1.36	1.50	1.74	1.87	1.95	1.96
GRU sup. [37]	0.28	0.57	0.90	1.02	-	-	-	-	0.32	0.63	1.07	1.26	-	-	-	-	0.52	0.89	1.25	1.40	-	-	-	-
DMGNN [32]	0.15	0.34	0.58	0.71	-	-	-	-	0.22	0.49	0.88	1.10	-	-	-	-	0.42	0.72	1.16	1.34	-	-	-	-
HistReptItself [34]	0.16	0.36	0.58	0.70	0.83	0.91	1.01	1.08	0.22	0.49	0.92	1.14	1.54	1.92	2.25	2.33	0.46	0.78	1.05	1.23	1.58	1.65	1.79	1.85
Ours W-Mean	0.13	0.34	0.58	0.70	0.78	0.83	0.89	0.97	0.20	0.46	0.88	1.09	1.46	1.77	2.05	2.11	0.41	0.71	1.15	1.32	1.52	1.69	1.77	1.79
Ours ML-Mode	0.14	0.34	0.57	0.70	0.79	0.84	0.88	0.96	0.20	0.45	0.87	1.08	1.46	1.77	2.06	2.12	0.41	0.72	1.16	1.33	1.53	1.71	1.79	1.83
milliseconds	Walk Together																							
	80	160	320	400	560	720	880	1000																
Zero Vel.	0.33	0.66	0.94	0.99	1.10	1.22	1.22	1.52																
GRU sup. [37]	0.27	0.53	0.74	0.79	-	-	-	-																
DMGNN [32]	0.15	0.33	0.50	0.57	-	-	-	-																
HistReptItself [34]	0.14	0.32	0.50	0.55	0.63	0.68	0.80	1.18																
Ours W-Mean	0.13	0.31	0.48	0.54	0.67	0.78	0.92	1.20																
Ours ML-Mode	0.13	0.31	0.49	0.55	0.70	0.81	0.98	1.27																

Table 8. Angle error on 8 samples per action on the H3.6M test dataset.

milliseconds	MPJPE [mm]							
	80	160	320	400	560	720	880	1000
Zero Vel.	23.8	44.4	76.1	88.3	107.5	121.6	131.6	136.6
HistReptItself [34]	12.4	25.9	51.4	62.5	81.4	96.3	108.6	116.4
HistReptItself 3D	11.3	24.1	49.9	60.8	78.3	92.0	105.1	112.8
Ours W-Mean	15.1	29.9	55.6	66.2	83.7	98.0	110.1	117.9
Ours ML-Mode	15.0	30.1	56.0	66.6	84.3	98.9	111.4	119.6
Ours Bo3-Modes	15.1	29.6	53.6	63.1	78.4	91.0	102.4	110.5
Ours Bo5-Modes	15.2	29.7	53.2	62.6	78.4	88.2	99.3	107.7

Table 9. Mean per Joint Position Error (MPJPE) on 256 samples per action on the H3.6M test dataset. HistReptItself 3D directly outputs 3D joint position and is therefore subject to bone deformation.

milliseconds	MPJPE [mm]					
	100	200	400	600	800	1000
Zero Vel.	41.9	72.9	106.2	115.3	115.3	112.5
HistReplItself [34]	20.4	39.8	64.4	74.8	80.5	85.8
Ours W-Mean	19.1	37.8	63.0	75.3	82.3	87.5
Ours ML-Mode	19.1	38.2	64.1	76.9	84.3	89.9
Ours Bo3-Modes	19.0	37.3	59.9	70.0	76.6	82.8
Ours Bo5-Modes	19.1	37.4	58.8	67.5	73.8	81.0

Table 10. Mean per Joint Position Error (MPJPE) on 10,000 samples from the AMASS test set.